ELSEVIER

Aerosol Science 35 (2004) 1235–1250

Journal of
Aerosol Science

www.elsevier.com/locate/jaerosci

Suppression of particle deposition in tube flow by thermophoresis

Jyh-Shyan Lin[a], Chuen-Jinn Tsai[a,*], Cheng-Ping Chang[b]

[a] *Institute of Environmental Engineering, National Chiao Tung University, No. 75 Poai St., Hsin Chu, Taiwan*
[b] *Institute of Occupational Safety and Health, Council of Labor Affairs, Taipei, Taiwan*

Received 20 February 2004; received in revised form 18 May 2004; accepted 26 May 2004

Abstract

Suppression of particle deposition from flow through a tube with circular cross-section was investigated numerically and experimentally for the case when the wall temperature exceeds that of the gas. Particle transport equations for convection, diffusion and thermophoresis were solved numerically to obtain particle concentration profiles and deposition efficiencies. The numerical results were validated by particle deposition efficiency measurements with monodisperse particles. For all particle sizes, the particle deposition efficiency was found to decrease with increasing tube wall temperature and gas flow rate. Particle deposition was suppressed completely when the tube wall was heated to a certain temperature slightly above that of the gas flow. An empirical expression has been developed to predict the dimensionless temperature difference needed for zero deposition efficiency in a laminar tube flow for a given dimensionless deposition parameter.

Keywords: Thermophoresis; Thermophoretic deposition; Particle sampling; Particle control

1. Introduction

Thermophoretic particle deposition in pipe flow (circular or annular) or in flow between parallel plates has been studied extensively (Chang, Ranade, & Gentry 1995; Tsai & Lu, 1995; Romay, Takagaki, Pui, & Liu 1998; He & Ahmadi, 1998; Santachiara, Prodi, & Cornetti 2002; Messerer, Niessner, & Pöschl 2003; Lin & Tsai, 2003; Tsai, Lin, Aggarwal, & Chen 2004). The parallel plate or annular tube geometry enables a high-temperature gradient to exist between two plates or annular

* Corresponding author. Tel.: +886-3-5731880; fax: +886-3-5727835.
E-mail address: cjtsai@mail.nctu.edu.tw (C.-J. Tsai).

0021-8502/$ - see front matter © 2004 Elsevier Ltd. All rights reserved.
doi:10.1016/j.jaerosci.2004.05.007

Nomenclature

c_p	specific heat capacity at constant pressure (kJ kg^{-1} K^{-1})
C	slip correction factor (dimensionless)
C_m	momentum exchange coefficient (dimensionless)
C_s	thermal slip coefficient (dimensionless)
C_t	temperature jump coefficient (dimensionless)
N	particle number concentration (1 m^{-3})
N_e	particle number concentration at inlet (1 m^{-3})
d_p	diameter of the particle (m)
D	particle diffusivity (m^2 s^{-1})
D_t	tube diameter (m)
e	elementary unit of charge (C)
k_g	gas thermal conductivity (W m^{-1} K^{-1})
k_p	particle thermal conductivity (W m^{-1} K^{-1})
K_E	a constant of proportionality (N m^2 C^{-2})
K_{th}	thermophoretic coefficient (dimensionless)
L	tube length (m)
n_p	particle charge (dimensionless)
Pe_g	gas Peclet number $(u_m \cdot r_0^2)/(\alpha \cdot L)$ (dimensionless)
Pr	gas Prandtl numer (dimensionless)
Q	inlet gas flow rate (m^3 s^{-1})
r	radial coordinate (dimensionless)
r_0	tube radius (m)
r_c	critical radial position (m)
Re	Reynolds number (dimensionless)
t	residence time (s)
T	gas temperature (K)
T_e	gas temperature at tube inlet (K)
T_w	wall temperature (K)
T_∞	free stream temperature (K)
$\vec{\nabla} T$	temperature gradient (K m^{-1})
u	gas velocity (axial direction) (m s^{-1})
u_m	average gas velocity (axial direction) (m s^{-1})
$\vec{V}_{th}$	thermophoretic velocity (m s^{-1})
z	axial coordinate (dimensionless)
z_{dep}	thermal entry length (m)
Z	dimensionless distance from the tube inlet $Z = z/(0.05 D_t\ Pe_g)$ (dimensionless)
Z_p	particle electrical mobility $Z_p = n_p e C/(3\pi v \rho_g d_p)$ (m^2 V^{-1} s^{-1})

Greek letters

α	thermal diffusivity $k_g/(\rho_g \cdot c_p)$ (m^2 s^{-1})
β_1	thermophoretic parameter $\beta_1 = Pr\ K_{th}(T_e - T_w)/T_w$ (dimensionless)

η	thermophoretic deposition efficiency (dimensionless)
η_c	particle deposition efficiency due to image force (dimensionless)
δ_{df}	dust free layer (m)
λ	mean free path of air molecules (m)
μ	dimensionless deposition parameter $\mu = \pi DL/Q$ (dimensionless)
ν	air kinematic viscosity (N s m^{-2})
θ	dimensionless temperature difference (dimensionless)
ρ_g	gas density (kg m^{-3})
ρ_p	particle density (kg m^{-3})

spaces by forced convection (Chang et al., 1995; Tsai & Lu, 1995), hence its thermophoretic particle deposition efficiency is higher than that of a circular tube geometry. It was found in our previous study (Lin & Tsai, 2003) that thermophoretic particle deposition occurs mostly near the tube inlet and the amount of particle deposition is higher for developing flow than for fully developed flow. The thermophoretic deposition efficiency in the laminar tube flow depends on three parameters, namely, the product of the Prandtl number and thermophoretic coefficient, $\mathrm{PrK_{th}}$, the dimensionless temperature $(T_e - T_w)/T_e$ and the gas Peclet number Pe_g. An empirical equation to predict thermophoretic deposition efficiency for circular tube flow was developed by Lin and Tsai (2003).

Thermophoretic deposition of aerosol particles is used not only in aerosol sampling but also in particle control. It was shown to be an efficient approach for filterless particle removal in diesel engine exhaust gas system (Shi & Harrison, 2001; Messerer et al., 2003). In addition, the thermophoretic coefficient of Waldmann's theory was found to be accurate for predicting the thermophoretic velocity both in the free molecular ($K_n > 1$) and transition ($K_n \approx 1$) regimes for agglomerate soot particles (Messerer et al., 2003).

In contrast to the extensive study on thermophoretic particle deposition, the number of studies on reducing particle deposition by thermophoretic force is limited to the deposition on wafer surfaces, e.g. by Stratmann, Fissan, Papperger, and Friedlander (1988), Ye et al. (1991) and Bae, Lee, and Park (1995). Stratmann et al. (1988) derived an expression for the thickness of the dust-free layer for flow over a free-standing wafer. As the temperature gradient at the wall and the velocity component normal to the wall were known, the particle equation of motion obtained from the equilibrium of inertial force, drag force and thermophoretic force on the particle was solved to find the thickness of the dust-free layer near the forward stagnation point of the wafer surface. According to Stratmann et al. (1988), the analytical expression of the dust free layer thickness is,

$$\delta_{df} = 0.961 \left(\frac{\nu}{a}\right)^{1/2} K_{th}^{1/2} \left[\frac{T_w - T_\infty}{T_w}\right]^{1/2} Pr^{0.189}. \quad (1)$$

The above equation states that the dust-free layer thickness depends on the temperature difference between the gas flow and wafer surface. However, there is no analytical solution available yet for thermophoretic particle deposition velocity at an arbitrary temperature difference. Based on Eq. (1), δ_{df} for aluminum and copper particles ($0.5 < d_p < 2$ μm) for a temperature difference as small as 10°C was found to range from 100 to 200 μm, which was thick enough to prevent particle deposition.

Ye et al. (1991) used the SIMPLER algorithm to solve the coupled Navier–Stokes, energy and convection–diffusion equations to obtain the velocity, temperature and concentration fields. The convection–diffusion equation took into account the external forces of sedimentation and thermophoresis. The measured particle deposition velocity on the wafer surface was found to decrease with an increasing temperature of the surface, and agree with the numerical results. It was shown that by heating the wafer surface to a temperature 10°C higher than the air flow, a clean zone between 0.03 to 1.0 μm particles was created. The experimental study of Bae et al. (1995) also showed that by raising the wafer surface temperature by 5°C higher than the surrounding air, the average deposition particle velocity in the range from 0.1 to 1 μm in diameter was reduced to less than 10^{-4} cm s^{-1}.

In contrast to the study of preventing particle deposition on wafer surface, there is no literature concerning the suppression of particle deposition in a tube flow. In practical application in the industry, such as in the semiconductor industry, a common practice is to heat up the tube wall to prevent particle deposition. However, the required wall temperature to effectively suppress particle deposition in the tube is unknown.

This study conducts numerical analysis to quantify particle deposition efficiency using different tube wall temperatures that are higher than the inlet gas flow temperature, under laminar tube flow conditions. The numerical results will then be verified with the experimental data. The numerical results will also be used to develop an empirical expression for predicting the minimum wall temperature needed to effectively suppress diffusional particle deposition by thermophoretic force.

2. Numerical method

In the present numerical simulation, the following fully developed flow field in a circular tube was used,

$$u(r) = 2u_{\mathrm{m}}\left[1 - \left(\frac{r}{r_0}\right)^2\right]. \tag{2}$$

The temperature field was obtained numerically from the following energy equation:

$$c_{\mathrm{p}}\nabla\cdot(\rho_{\mathrm{g}}\,\vec{u}\,T) = \nabla\cdot(k_{\mathrm{g}}\nabla T), \tag{3}$$

where the boundary conditions are

$$T(r,0) = T_{\mathrm{e}}; \quad T(r_0,z) = T_{\mathrm{w}}; \quad \frac{\partial T}{\partial r}(0,z) = 0. \tag{4}$$

Particle concentration field was obtained numerically by solving the following particle convection–diffusion equation:

$$\nabla\cdot(\vec{u}\,N) = \nabla\cdot(D\nabla N) - \nabla\cdot(\vec{V}_{\mathrm{th}}N), \tag{5}$$

where $\vec{V}_{\mathrm{th}}$ is the particle thermophoretic velocity defined as,

$$\vec{V}_{\mathrm{th}} = -\frac{\nu K_{\mathrm{th}}}{T}\,\vec{\nabla}\,T \tag{6}$$

with the following boundary conditions:

$$N(r,0)=N_e; \quad N(r_0,z)=0; \quad \frac{\partial N}{\partial r}(0,z)=0. \tag{7}$$

In Eq. (5) the following thermophoretic coefficient K_{th} proposed by Talbot, Cheng, Schefer, and Willis (1980) was used:

$$K_{th}=\frac{2C_sC}{(1+3C_m(2\lambda/d_p))}\times\left(\frac{k_g/k_p+C_t(2\lambda/d_p)}{1+2(k_g/k_p)+2C_t(2\lambda/d_p)}\right). \tag{8}$$

This equation for the thermophoretic coefficient has been found to be accurate (Tsai & Lu, 1995; Messerer et al., 2003; Tsai et al., 2004).

The energy and particle convection–diffusion equations were solved by the finite difference method using SIMPLE algorithm (Patankar, 1980). In the test run, three different numbers of grids in the computational domain: 4000 (100 in the axial direction × 40 in radial direction), 12,000 (200 in the axial direction × 60 in radial direction) or 25,200 (280 in the axial direction × 90 in radial direction) were used. The cell spacing was set to be finer near the wall and inlet where the temperature gradients in the radial direction were expected to be larger. The numerical results showed that the number of grid of 12,000 was accurate enough and was adopted in the further study.

3. Experimental method

The experimental setup is shown in Fig. 1. The experimental system is similar to that described in Tsai et al. (2004). It consists of the aerosol generation and conditioning section, experimental section and temperature, flow and particle measurement system. The tube length of the conditioning and experimental section are 1.56 and 1.18 m, respectively, with an inner tube diameter of 0.0043 m. The test flow rates were 2, 3 and 5 slpm with the corresponding flow Reynolds number of 640, 960 and 1600.

The aerosol was generated by a constant output atomizer (TSI model 3076) and mixed with dry clean air in a mixing tank. Then it was passed through a silica gel diffusion dryer. After being dried, the aerosol was neutralized by a TSI 3077 electrostatic charge neutralizer. Particles of a known electrical mobility were then selected by a differential mobility analyzer (TSI 3081 Long DMA column). The monodisperse aerosol from the DMA was neutralized again and mixed with clean dilution air in another mixing tank to conduct experiment for particles in Boltzmann charge equilibrium. For the experiment involving only completely charge neutral (or zero charge) particles, an electrical condenser was used between the neutralizer and mixing tank to remove all charged particles.

In the conditioning section, the monodisperse aerosol stream was passed through a heat exchanger with a thermostated silicone–oil bath to keep the stream at a constant temperature of 296 K. In the experimental section, the tube wall was heated to the desired temperature from 296 to 315 K by another heat exchanger with a thermostated water bath to establish a temperature difference between the gas and the tube wall for the particle deposition suppression experiment.

Three thermocouples installed at the inlet of conditioning section, the outlet of the experimental section, and the junction between the conditioning section and experimental section were used to monitor the temperature of the aerosol stream. The flow rate of the aerosol flow from the experimental

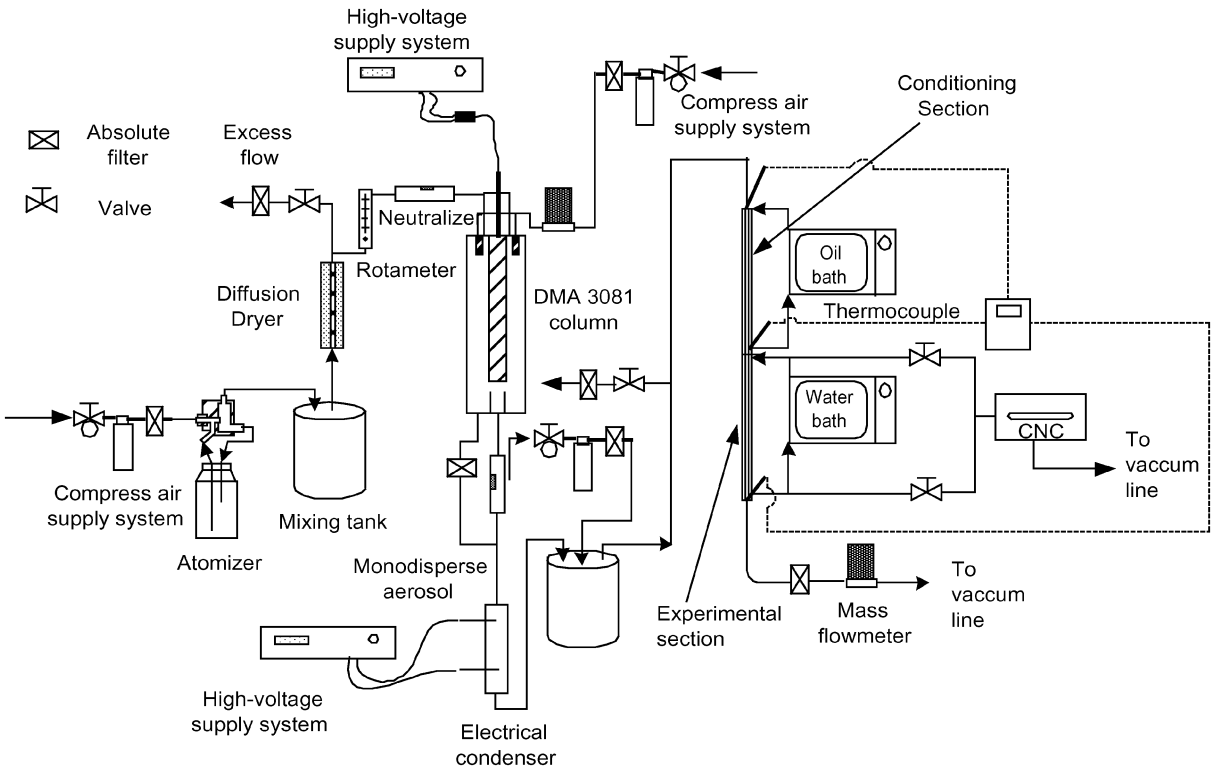

Fig. 1. The schematic diagram of the experimental setup.

section was set by a downstream mass flow controller (MKS model 1179A). The aerosol number concentrations at the inlet and outlet of the experimental section were measured using a TSI 3760 clean room condensation nucleus counter (CNC) with sampling flow rate of $1.5\,\mathrm{l\,min^{-1}}$.

The particles used in this study were NaCl or oleic acid generated from 1.0% w/v aqueous NaCl solution or 2%, v/v oleic acid dissolved in alcohol. The flow rate of the sheath air and polydisperse aerosol stream of the DMA was kept constant at 5 and $0.5\,\mathrm{l\,min^{-1}}$, respectively, throughout the experiment.

The particle deposition efficiency at a certain flow rate and particle diameter was determined from the particle number concentration data at the inlet and outlet of the experimental section. The deposition efficiency due to pure laminar flow convection diffusion was first obtained when the tube wall and aerosol stream were both kept at the temperature of 296 K, the so-called isothermal case. Then the tube wall temperature was raised to a desired temperature for determining the reduced deposition efficiency due to thermophoresis. The test was repeated for different flow rates and particle sizes. One data point at a particular test condition and particle diameter was the average of 6–8 efficiency measurements, while each measurement consisted of 10 particle concentration readings at the inlet and the outlet, respectively. The measurement time was about 2 min per 10 readings excluding the system stabilization time, which was varied anywhere from 20–100 s/reading. After the completion of one efficiency measurement, the experimental section was purged clean by passing clean air through it before the next measurement was started.

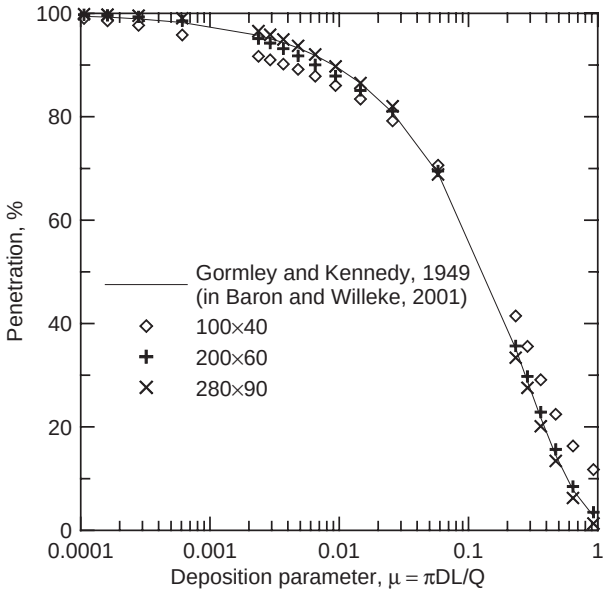

Fig. 2. Particle deposition efficiency as a function of dimensionless parameter, $\mu = \pi DL/Q$, for isothermal case.

4. Results and discussion

4.1. Effect of grid number on the particle deposition efficiency

The particle convection–diffusion equation, Eq. (5), without considering thermophoresis was solved and the numerical diffusional efficiency was compared with Gormley and Kennedy equation (Baron & Willeke, 2001). This is the so-called isothermal case when the tube wall and inlet gas flow temperatures are the same. Fig. 2 shows the particle deposition efficiency as a function of the dimensionless deposition parameter, $\mu = \pi DL/Q$, based on different numbers of grids. It is seen that the numerical method is able to predict the particle deposition efficiency due to convention–diffusion in a tube flow very well. As the number of grids is increased from 4000 to 12,000 or 25,200, the accuracy of the numerical prediction is also improved. At the grid number of 12,000, the calculated deposition efficiency was found to be accurate and deviate from the analytical value by a maximum of 1.9% only. Hence in the subsequent study, the grid number of 12,000 is used.

4.2. Thermophoretic deposition efficiency

To make sure that the present numerical study is accurate, the thermophoretic deposition efficiency was calculated based on fully developed flow assumption. The simulated thermophoretic deposition efficiency in laminar tube flow shown in Fig. 3 illustrates that the present numerical results agree with the exact solution of Walker, Homsy, and Geyling (1979) or semi-empirical equation of Lin and Tsai (2003). The approximate equation of Walker et al. (1979) slightly underestimated the

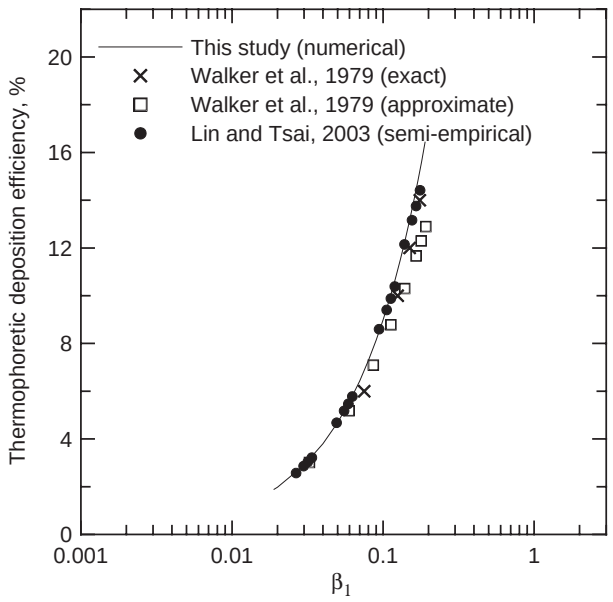

Fig. 3. Dimensionless temperature profiles as a function of dimensionless radial and axial coordinates. *The exact solutions of Walker et al. (1979) were taken from Table 3 of their paper.

thermophoretic deposition efficiencies, it is given in the following as,

$$\eta = \frac{Pr\ K_{\mathrm{th}}}{T_{\mathrm{w}}}(T_{\mathrm{e}} - T_{\mathrm{w}}), \tag{9}$$

Hence, both the isothermal convection–diffusion results in the last section, and thermophoretic deposition efficiency results in this section demonstrate that the present numerical simulation is accurate.

4.3. Effect of temperature difference between the tube and gas flow on the particle deposition efficiency

The effect of heating up the tube wall on reducing particle deposition efficiency was studied both numerically and experimentally. The inlet air flow temperature at the experimental section was kept constant at 296 K while the tube wall temperature was increased from 296 to 315 K. Three aerosol flow rates of 2, 3 and 5 slpm with the corresponding Reynolds number of 640, 960 and 1600, respectively, were tested using particles ranging from 0.01 to 0.04 μm in diameter. Figs. 4(a)–(c) show the comparison between the numerical and experimental results for NaCl particles with the diameter of 0.01, 0.02 and 0.04 μm, respectively. The experimental data show good agreement with numerical results in these figures. It is seen that for a given particle diameter, the particle deposition efficiency is decreased with an increasing tube wall temperature and gas flow Reynolds number. Reduction of deposition efficiency is very steep when the tube wall is only several degrees higher than the air flow temperature. The deposition of particle is suppressed completely (or zero deposition

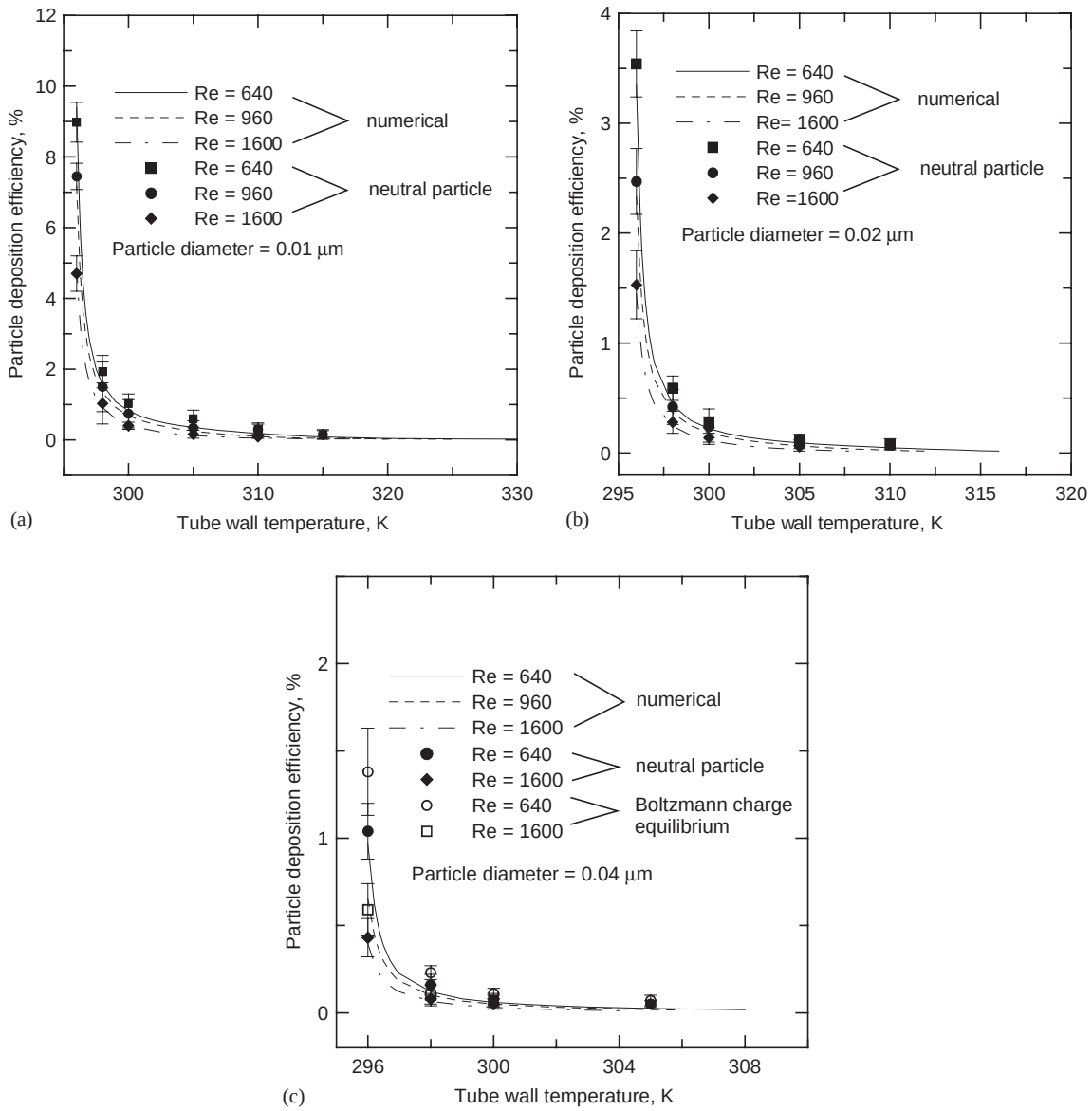

Fig. 4. Particle deposition efficiency versus tube wall temperature for NaCl particles with particle diameter of (a) 0.01 μm (b) 0.02 μm (c) 0.04 μm. The test tube length and inner diameter are 1.18 and 0.0043 m, respectively, and the inlet air temperature is 296 K.

efficiency) when the tube wall is heated to a temperature high enough so that diffusional force is overcome by thermophoretic force.

Fig. 4(a) illustrates that the numerical results of a 0.01 μm NaCl particle at charge neutral condition, the numerical particle deposition efficiencies are 9.39%, 7.19% and 4.88% at the corresponding gas flow rate of 2, 3 and 5 slpm, respectively, when the tube wall temperature is kept at 296 K.

These are laminar diffusion efficiencies. Further increasing the tube wall temperature to 320, 315 and 312 K for the gas flow rate of 2, 3 and 5 slpm, respectively, the particle deposition efficiency will drop to zero.

Increasing the particle diameter to 0.02 or 0.04 μm, similar effect of wall temperature on reducing deposition efficiency can be observed in Figs. 4(b) and (c). For 0.02 μm particles (Fig. 4(b)) and when tube wall is kept at 296 K, the numerical particle deposition efficiencies are 3.35%, 2.33% and 1.45% at the gas flow rate of 2, 3 and 5 slpm, respectively. Zero particle deposition efficiency occurs at the tube wall temperature of 312, 308 and 305 K for the gas flow rate of 2, 3 and 5 slpm, respectively. For 0.04 μm particles (Fig. 4(c)), zero particle deposition efficiency occurs as the tube wall is increased to 304, 302 and 300 K for the gas flow rate of 2, 3 and 5 slpm, respectively. That is, increasing the particle diameter will reduce the convection–diffusion strength of particles, and hence the required wall temperature for zero deposition is also decreased.

The above data are for completely charged neutral particles. For particles in Boltzmann charge equilibrium, the experimental results for 0.04 μm particles are shown in Fig. 4(c), which shows that deposition efficiency is slightly higher (less than 0.34% in average) than that of charge neutral particles. This is due to the image force exerted on the particles that carry charges. Yu and Chandra (1978) derived the following equation for calculating the critical particle radius, r_c, for the fully developed circular tube flow:

$$\frac{r_0}{r_c} + 2\ln\frac{r_c}{r_0} - \left(\frac{r_c}{r_0}\right)^2 + \frac{1}{3}\left(\frac{r_c}{r_0}\right)^3 - \frac{1}{3} = \frac{Z_p K_E n_p e t}{D_t^3} \tag{10}$$

All particles starting at the tube entrance with $r > r_c$ will deposit on the tube wall. The particle deposition efficiency is,

$$\eta_c = \left(1 - \left(\frac{r_c}{r_0}\right)^2\right)^2. \tag{11}$$

The calculated particle deposition efficiency due to image force for a singly charged particle is 0.057% ($Re = 1600$) or 0.059% ($Re = 640$) when the tube wall temperature is the same as that of the gas flow, 296 K. Considering that the singly charged fraction (positive or negative) is 34.4% for 0.04 μm particles, the theoretical particle deposition efficiency due to image force for the particles in Boltzmann charge equilibrium is 0.019% ($Re = 1600$) or 0.020% ($Re = 640$). That is, the theoretical calculation also shows that the electrostatic effect does not increase the deposition efficiency for particles in Boltzmann charge equilibrium.

The deposition efficiency data show little difference between oleic acid and NaCl particles. That is, particle material has no effect on particle deposition efficiency. This is expected as the Knudsen number is greater than 3, the thermophoretic coefficient will remain constant at 0.55 and is independent of particle conductivity (Tsai et al., 2004; Messerer et al., 2003). In this study, Kn ranges from 3.3 to 13.5. Therefore, tube wall temperature needed to completely suppress particle deposition of a given particle size is the same for different particle materials.

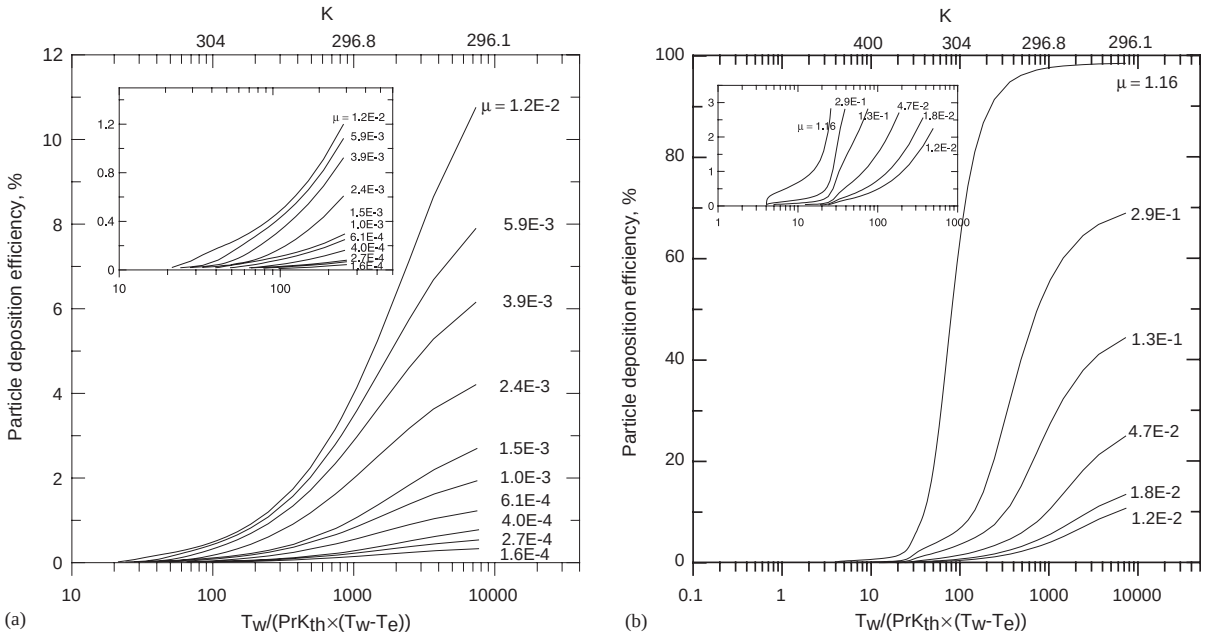

Fig. 5. Particle deposition efficiency as a function of the dimensionless temperature difference, $T_w/(Pr\ K_{th}(T_w - T_e))$, and deposition parameter, $\pi DL/Q$. Dimensionless deposition parameter is (a) from 1.6×10^{-4} to 1.2×10^{-2} and (b) from 1.2×10^{-2} to 1.16. (Insets in the figures are deposition efficiency curves near zero deposition efficiency. For air and current tube geometry and length, the corresponding wall temperature is marked in the upper x-axis.)

4.4. Particle deposition efficiency versus dimensionless temperature difference and deposition parameter

The particle deposition efficiency can be plotted as a function of the dimensionless temperature difference, $\theta = T_w/(Pr\ K_{th}(T_w - T_e))$, and laminar diffusional deposition parameter, $\pi DL/Q$, as shown in Figs. 5(a) and (b). The dimensionless temperature difference is the negative of the inverse thermophoretic parameter. The deposition parameter μ ranges from 1.6×10^{-4} to 1.2×10^{-2} and 1.2×10^{-2} to 1.16 in Figs. 5(a) and (b), respectively, to cover the entire range of μ. It is shown that when μ is small and less than 1.2×10^{-2} (Fig. 5(a)), the deposition efficiency is less than 11%, in the range of dimensionless temperature difference (10–1000) studied. The deposition efficiency is seen to decrease monotonically to zero as the dimensionless temperature difference is decreased from 7600 to less than 70. Whereas in Fig. 5(b), when μ ranges from 1.2×10^{-2} to 1.16, the deposition efficiency ranges from 0% to 100%. It is seen that when μ is larger and closer to 1, the particle deposition efficiency is decreased more sharply with a decreasing $T_w/(Pr\ K_{th}(T_w - T_e))$. Zero particle deposition is achieved when $T_w/(Pr\ K_{th}(T_w - T_e))$ is smaller than a certain value. To obtain the required dimensionless temperature difference for zero deposition efficiency, wall temperature was gradually increased until the deposition efficiency was reduced below about 0.04%, which was the smallest achievable efficiency in the current simulation. Then the simulation was ceased.

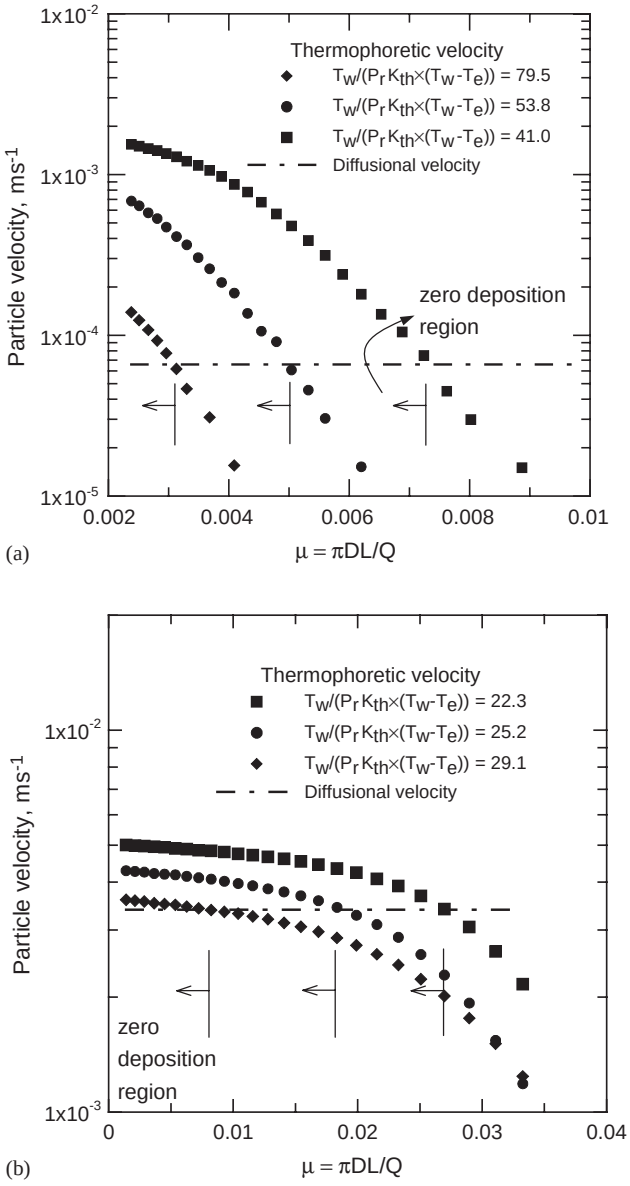

Fig. 6. The variation of radial particle thermophoretic and diffusional velocities in the axial direction as the tube wall is heated at various temperatures at a given particle diameter of (a) 0.02 μm (b) 0.005 μm and a constant flow rate of 1 l min^{-1}.

The radial thermophoretic and diffusional velocities of aerosol particles were calculated by evaluating the temperature and concentration gradients at the tube wall, respectively, at different axial positions, as shown in Fig. 6. For the parameter μ in the figures, L is increased while D and Q are fixed. The diffusional velocity evaluated at the tube wall is seen to remain constant in the axial

direction while the thermophoretic velocity curves are different for three different heated wall temperatures, and a higher wall temperature gives rise to a higher particle thermophoretic velocity. For a fixed $T_w/(Pr\ K_{th}(T_w - T_e))$, when the radial thermophoretic velocity is higher than the diffusional velocity, particles will not deposit on the tube wall. This normally occurs near the entrance or the front part of the tube, or when L is less than a certain value assuming Q and D are fixed. Beyond that, the gas flow is heated to a temperature close to the wall temperature, such that the thermophoretic velocity drops below the diffusional velocity and particle deposition will occur again. That is, if the entire tube is heated, thermophoresis is only effective to suppress particle deposition for a certain front section of the tube only. The effective length depends on the particle diameter, flow rate, and $T_w/(Pr\ K_{th}(T_w - T_e))$. For example in Fig. 6(a), when $T_w/(Pr\ K_{th}(T_w - T_e))$ is 79.5, 53.8 and 41.0, the zero deposition region corresponds to μ values less than 3.1×10^{-3}, 5.0×10^{-3} and 7.2×10^{-3}, respectively. Similarly in Fig. 6(b), when $T_w/(Pr\ K_{th}(T_w - T_e))$ is 22.3, 25.2 and 29.1, the zero deposition region corresponds to μ values less than 8.2×10^{-3}, 1.18×10^{-2} and 2.7×10^{-2}, respectively.

Furthermore, as the temperature of the tube wall is heated slightly higher than that of the inlet gas flow, the radial concentration profiles along the axial direction can be shown to be quite different from the isothermal case. For example in the isothermal case, for a particle diameter of 0.005 μm, the convection–diffusion is strong and the deposition efficiency due to pure laminar diffusion is 28% for the current tube geometry and length when $\mu = 0.015$ (corresponding flow rate is 5 slpm, $Re = 1600$, tube ID is 0.0043 m, and length is 1.18 m). The dimensionless particle concentration profile near the wall is changed into more parabolic shape in an increasing dimensionless axial coordinate Z, as shown in Fig. 7(a). In contrast, when the tube wall is heated slightly higher than the inlet gas temperature by 2 K, the concentration profile has a much steeper slope near the wall and does not change very much in the axial direction. This dictates a constant concentration gradient and constant radial diffusional velocity (evaluated at the wall) in the axial direction as shown in Fig. 6. The deposition efficiency is also much smaller than the isothermal case. The wall temperature needed to suppress particle deposition completely is 327 K, and the corresponding dimensionless concentration profiles are also given in Fig. 7(a). The radial temperature profiles along the axial direction are shown in Fig. 7(b) when the tube wall is heated to 298 K. It can be seen that the temperature gradient is very high near the wall at the tube entrance and gradually decreases as the tube length increases. The high-temperature gradient results in thermophoretic force that is high enough to overcome diffusional force and prevent particle deposition at the tube entrance. However, beyond a certain axial distance, the temperature gradient may drop below a value that is not high enough to suppress particle deposition.

4.5. An equation to predict the dimensionless temperature difference needed for zero particle deposition

A fitted equation to predict the dimensionless temperature difference needed for complete suppression of particle deposition can be obtained from the curve fitting of the present numerical results. The dimensionless temperature difference, $\theta = T_w/(Pr\ K_{th}(T_w - T_e))$, needed for zero deposition is plotted versus the dimensionless deposition parameter $\mu = \pi DL/Q$, as shown in Fig. 8. The region below and to the left of the curve is the zero particle deposition region. It is seen that θ decreases (or T_w increases) sharply with respect to an increasing μ (increasing diffusional strength). For example,

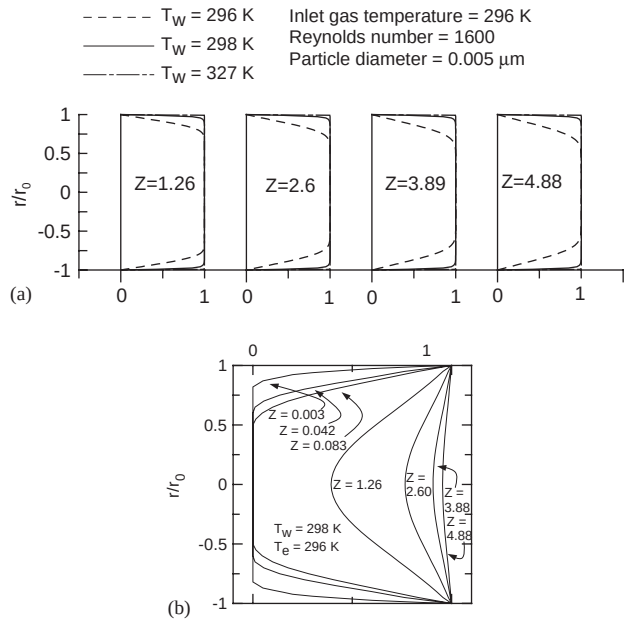

Fig. 7. (a) Dimensionless radial concentration profiles and (b) dimensionless radial temperature profiles as a function of dimensionless axial coordinates. The test tube length and inside diameter are 1.18 and 0.0043 m, respectively.

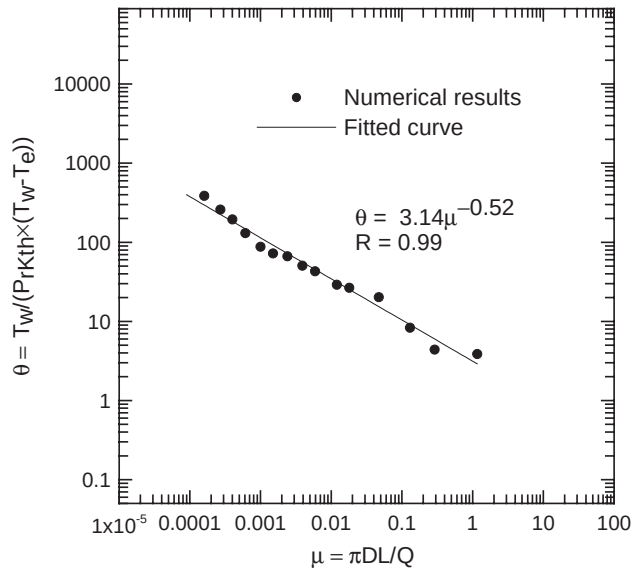

Fig. 8. The relationship between the required dimensionless temperature difference, $\theta = T_w/(Pr\ K_{th}(T_w - T_e))$, and the dimensionless deposition parameter, $\mu = \pi DL/Q$, for zero particle deposition for a circular tube air flow. Symbols represent the numerical results and the solid line is the fitted curve.

θ is 343.4 when μ is 1.2×10^{-4} and it drops to 120.5 when μ is increased to 9.0×10^{-4}. The best fit to the numerical data can be expressed as

$$\theta = 3.14\mu^{-0.52}, \quad 1.6 \times 10^{-4} < \mu < 1.0. \tag{12}$$

The above expression is useful for predicting the minimum wall temperature needed to achieve zero deposition efficiency in a laminar tube flow for any dimensionless deposition parameter. For example, for particles of 0.02 μm in diameter suspended in the tube flow with the flow rate of 0.5 slpm and inlet temperature of 320 K, the calculated μ value is 6.1×10^{-3} for the present tube geometry and length (ID = 0.0043 m, $L = 1.18$ m). The θ value for complete suppression of particle deposition is 44.2, which corresponds to a minimum wall temperature of 340 K.

5. Conclusions

Suppression of particle deposition by thermophoresis in laminar tube flow was investigated numerically in this study. The numerical results were validated by the experimental data obtained in this study. It was found that a sharp reduction of particle deposition efficiency occurs as the tube wall is heated to a temperature slightly higher than that of the gas flow. Complete suppression, or zero particle deposition is achieved when $T_w/(Pr\ K_{th}(T_w - T_e))$ is less than a certain value, which is determined solely by μ, the dimensionless deposition parameter. The effective region to suppress particle deposition completely occurs near the front section of the tube where temperature difference exists between the tube wall and the flow. Beyond that region, particle deposition occurs again when the flow is gradually heated to a certain temperature such that particle thermophoretic force is reduced below the diffusional force.

An empirical expression has been developed to calculate the dimensionless temperature difference, or the minimum wall temperature, needed for zero particle deposition for a given dimensionless deposition parameter ranging from 1.6×10^{-4} to 1.0.

Acknowledgements

The authors would like to thank the Taiwan National Science Council for the financial support of the project NSC 92-2211-E-009-037.

References

Bae, G. N., Lee, C. S., & Park, S. O. (1995). Measurements and control of particle deposition velocity on a horizontal wafer with thermophoretic effect. *Aerosol Science Technology*, *23*, 321–330.

Baron, P. A., & Willeke, K. (2001). *Aerosol measurement*: *Principles*, *techniques and applications* (pp. 174). New York: Wiley.

Chang, Y. C., Ranade, M. B., & Gentry, J. W. (1995). Thermophoretic deposition in flow along an annular cross section: Experiment and simulation. *Journal of Aerosol Science*, *26*, 407–428.

He, C., & Ahmadi, G. (1998). Particle deposition with thermophoresis in laminar and turbulent duct flows. *Aerosol Science Technology*, *29*, 525–546.

Lin, J.-S., & Tsai, C.-J. (2003). Thermophoretic deposition efficiency in a cylindrical tube taking into account developing flow at the entrance region. *Journal of Aerosol Science*, *34*, 569–583.

Messerer, A., Niessner, R., & Pöschl, U. (2003). Thermophoretic deposition of soot aerosol particles under experimental conditions relevant for modern diesel engine exhaust gas systems. *Journal of Aerosol Science*, *34*, 1009–1021.

Patankar, S. V. (1980). *Numerical heat transfer and fluid flow*. New York: McGraw-Hill.

Romay, F. J., Takagaki, S. S., Pui, D. Y. H., & Liu, B. Y. H. (1998). Thermophoretic deposition of aerosol particles in turbulent pipe flow. *Journal of Aerosol Science*, *29*, 943–959.

Santachiara, G., Prodi, F., & Cornetti, C. (2002). Experimental measurements on thermophoresis in the transition region. *Journal of Aerosol Science*, *33*, 769–780.

Shi, J. P., & Harrison, R. M. (2001). Study of a water-cooled fluidized bed for diesel particle agglomeration. *Powder Technology*, *115*, 146–156.

Stratmann, F., Fissan, H., Papperger, A., & Friedlander, S. (1988). Suppression of particle deposition to surfaces by the thermophoretic force. *Aerosol Science Technology*, *9*, 115–121.

Talbot, L., Cheng, R. K., Schefer, R. W., & Willis, D. R. (1980). Thermophoresis of particles in a heated boundary layer. *Journal of Fluid Mechanics*, *101*, 737–758.

Tsai, C.-J., Lin, J.-S., Aggarwal, S. G., & Chen, D.-R. (2004). Thermophoretic deposition of particles in laminar and turbulent tube flows. *Aerosol Science Technology*, *38*, 131–139.

Tsai, C.-J., & Lu, H.-C (1995). Design and evaluation of a plate-to-plate thermophoretic precipitator. *Aerosol Science Technology*, *22*, 172–180.

Walker, K. L., Homsy, G. M., & Geyling, R. T. (1979). Thermophoretic deposition of small particles in laminar tube flow. *Journal of Colloid Interface Science*, *69*, 138–147.

Ye, Y., Pui, D. Y. H., Liu, B. Y. H., Opiolka, S., Blumhorst, S., & Fissan, H. (1991). Thermophoretic effect of particle deposition on a free standing semiconductor wafer in a clean room. *Journal of Aerosol Science*, *22*, 63–72.

Yu, C. P., & Chandra, K. (1978). Deposition of charged particles from laminar flows in rectangular and cylindrical channels by image force. *Journal of Aerosol Science*, *9*, 175–180.